BOREAL ENVIRONMENT RESEARCH 17: 327–346
ISSN 1239-6095 (print) ISSN 1797-2469 (online)

Helsinki 28 September 2012

Relationship between Eurasian large-scale patterns and regional climate variability over the Black and Baltic Seas

Gintautas Stankūnavičius[1)], Dmitry Basharin[2)] and Donatas Pupienis[1)]

[1)] *Department of Hydrology and Climatology, Vilnius University, Čiurlionio 21/27, LT-01513 Vilnius, Lithuania*
[2)] *Sevastopol Marine Hydrophysical Institute, National Academy of Science of Ukraine, Kapitanskaya Street 2, Sevastopol 99011, Ukraine*

Received 16 May 2011, final version received 24 Jan. 2012, accepted 16 Dec. 2011

Stankūnavičius, G., Basharin, D. & Pupienis, D. 2012: Relationship between Eurasian large-scale patterns and regional climate variability over the Black and Baltic Seas. *Boreal Env. Res.* 17: 327–346.

Using a NCEP/NCAR Reanalysis dataset and the empirical orthogonal function (EOF) analysis approach we studied interannual to decadal variabilities of the sea-level air pressure (SLP) and the surface air temperature (SAT) fields over Eurasiaduring the 2nd part of the 20th century. Our results agree with those of the previous studies, which conclude that Eurasian trends are the result of storm-path changes driven by the interdecadal behaviour of the NAO-like meridional dipole pattern in the Atlantic. On interannual and decadal time scales, significant synchronous correlations between correspondent modes of SAT and SLP EOF patterns were found. This fact suggests that there is a strong and stable Eurasian interrelationship between SAT and SLP large-scale fields which affects the local climate of two sub-regions: the Black and Baltic Seas. The climate variability in these sub-regions was studied in terms of Eurasian large-scale surface-temperature and air-pressure patterns responses. We concluded that the sub-regional climate variability substantially differs over the Black and Baltic Seas, and depends on different Eurasian large-scale patterns. We showed that the Baltic Sea region is influenced by the patterns arising primary from NAO-like meridional dipole, as well as Scandinavian patterns, while the Black Sea's SAT/SLP variability is influenced mainly by the second mode EOF (eastern Atlantic) and large scale tropospheric wave structures.

Introduction

Changes in surface air temperatures (SAT) and pressure fields are the most popular indices used in global and regional climate change detection. Relationships between mean SAT patterns and regional or hemispheric circulation indices show significant differences between seasons. The strong dependency of northern Eurasia wintertime SAT on the intensity of large-scale zonal flow variations, which are best represented by indices of the North Atlantic and/or Arctic oscillations (NAO and AO, respectively), has already been well documented (Rogers 1997, Thompson *et al*. 2000, Slonsky and Yiou 2002, Kryjov 2004, Savelieva *et al*. 2004). In addition, these processes have the greatest influence on the most recurrent sea-level air pressure (SLP) and SAT patterns in shape and persistency that are usually represented by the first modes of empirical

Editor in charge of this article: Hannele Korhonen

orthogonal functions (EOF) of these fields in almost all seasons (Barnston and Livezey 1987, Brönnimann *et al*. 2009). Also, there are certainly many other patterns that are important and persistent in particular seasons. For example, the Scandinavian pattern is an important factor for storminess over Scandinavia and northeastern Europe from autumn to spring. It is reminiscent of a wave train and has been linked to tropical convection via Rossby wave propagation (Seierstad *et al*. 2007).

The most generalized study concerning atmospheric circulation patterns and their dynamic connection to the temperature anomalies across Europe was presented by Philipp *et al*. (2007). Jones and Lister (2009) continued this research by including precipitation and diurnal temperature range, which produced circulation types. Nonetheless, these hydrometeorological fields of the interannual-decadal variations at the global and regional scales were still not able to be accurately simulated [within the Coupled Model Intercomparison Project (CMIP3)] (Jamison and Kravtsov 2010, Polonsky *et al*. 2011). Moreover, some authors argued that large scale atmospheric circulation changes took place in the 1970s and have changed also the European climate (Pekarova *et al*. 2006). That effect was partly explained by the relative stability and intensification of the NAO, which is dominant during most of the year (Savelieva *et al*. 2004, Basharin 2009). Others attribute such changes to the last decade of the last century, when the persistent positive Arctic Oscillation phase became dominant and consequently had an impact on the Arctic sea ice reduction and the following positive feedback to the atmospheric fields (Honda *et al*. 2009, Overland and Wang 2010).

All described main modes of large-scale variability result in a different regional European response. Therefore, some studies tried to correlate the formation of the regional and local temperature and/or precipitation anomalies with circulation types, air pressure patterns or regional and hemispheric circulation indices. The most extensive study, comprising the larger part of Europe in the winter season, was presented by Beranová and Huth (2008). They maintained that the winter circulation contributes mostly to the annual temperature and precipitation (in some regions). This was also shown by Kryjov (2004).

However, earlier studies have shown that NAO has a definite influence on precipitation but weak links to temperature in southern Europe, while opposite effects were observed in central and eastern Europe; NAO also has strong links to both temperature and precipitation in northern Europe (Hurrell and van Loon 1997, Castro-Diez *et al*. 2002). Thus, the present study will focus on the climate variability of the two sub-regions in northern and southern Europe, which are dependent on Eurasian large-scale patterns. It is induced not only by the phase of the NAO, but also the exact location of the NAO center (Castro-Diez *et al*. 2002). Therefore, different available indices of NAO-like meridional dipole pattern over the North Atlantic are worth taking into consideration.

Regional climate studies focused on the southeastern Baltic region as a whole (Jaagus *et al*. 2009, 2010), as well as on a local scale (Degirmendzic *et al*. 2004, Bukantis and Bartkevičienė 2005, Niedźwiedź *et al*. 2009, Stankunavičius 2009), dealt with various aspects of climate variability: air temperature and precipitation anomaly predictability, climate extremes and climate change diagnostics using circulation indices and patterns, air pressure pattern stability and its link to weather anomalies, etc. In atmospheric-circulation studies, the Black Sea region is considered either a part of the larger eastern Mediterranean climatic region (Kutiel *et al*. 1996, Kutiel and Benaroch 2002, Krichak and Alpert 2005), or a part of the different states surrounding the Black Sea (Turkes 1998, Efimov *et al*. 2002, Tomozeiu *et al*. 2005, Sizov and Chekhlan 2007). Influence of seas on the regional hydrometeorological variability over the sub-regions we selected brings additional noise. Also, these sub-regions are frequently divided by zero isolines in the leading patterns, presuming the opposite local effects on southern and northern Europe. However, there are still months when the sub-regions are not divided by zero isolines in the leading patterns (Barnston and Livezey 1987). All of these listed facts complicate investigations of the local sub-regions' climate variability.

The priority in the analysis of the regional and/or hemispheric scale circulation (e.g. North Atlantic-European) and its impact on the local or

regional weather, as is often the case in scientific papers, has been put on well recognized indices (e.g., NAO). Jahnke-Bornemann and Brümmer (2009) argued that well documented and widely used circulation indices, like NAO, do not always strictly pertain to the bipolar structure of two centers of action. They show that the northeast Atlantic elongated low air-pressure zone is actually represented by two separate air-pressure centers that could act in phase or out of phase, and consequently produce different temperature anomalies over large territories. Also, such behavior of different parts of single centers of action affects other prominent northern-hemisphere air-pressure centers: the Aleutian/Island low and the Siberian/Azores/Hawaii high.

The objective of the paper is to assess the regional temperature and precipitation variability in two sub-regions (the Black and Baltic Seas) against the background of the large-scale Eurasian temperature and air-pressure patterns and their relation to the regional and hemispheric circulation indices.

Material and methods

Monthly air temperature and sea-level air-pressure NCEP/NCAR reanalysis data on a regular grid for the 1950–2001 period were used in the large-scale pattern extraction procedure. Spatial resolution for temperature was 1.875° × 1.875° latitude/longitude and for sea-level air-pressure 2.5° × 2.5° latitude/longitude. For the purpose of this study, the Eurasian region was considered to be located between 27.5°–80°N and 12.5°W–152.5°E.

The following two sub-regions were selected to determine the local response to large-scale spatial temporal structures: the southeastern Baltic and northern Black Sea. Each area is represented by three meteorological stations: Klaipėda, Visby, Łeba; and Odessa, Yevpatoriya, Kerch; respectively (Fig. 1A). All stations are located near the open sea (within 0.1–5 km from the coastline). None of the listed stations experience orographic effect on meteorological fields. Monthly mean air temperatures at the 2-m level were obtained for Łeba (1950–2001), Visby (1950–2001), Odessa (1950–2001), and Kerch (1976–2001) from the European Climate Assessment & Dataset (ECA&D) project. These data are freely available from http://eca.knmi.nl/. Monthly mean air temperatures at the 2-m level for Yevpatoriya (1950–2001) and Kerch (1950–1975) were obtained from hydrometeorological services, and for Visby and Łeba (1950–2001) from KNMI Climate Explorer(http://climexp.knmi.nl/). Since Kerch station's monthly temperature data series were combined from two different sources, the homogeneity test was applied to the newly constructed temperature data series. Kerch's temperature series was concluded to be homogenous at $p < 0.05$.

Precipitation data in this study were obtained from a gridded database due to the large spatio-temporal variability of the precipitation data of coastal stations, which are affected by different types of breeze circulation and airflow divergence near the seashore. Monthly precipitation series were extracted from the Global Precipitation Climatology Centre (GPCC) dataset with the 0.5° spatial resolution (ftp://ftp-anon.dwd.de/pub/data/gpcc/). The selected Full Data Product covers the period from 1901 to 2010, based on quality controlled data from a greater number of stations with irregular coverage in time. This product is optimized for the best spatial coverage and used for water budget studies (Rudolf *et al*. 2011). For all analyzed meteorological stations, the following six different grid-point series having the highest Pearson's correlations (r_p) with the precipitation data series were selected from the GPCC archive: 56.2°N, 21.2°E for Klaipėda, 57.2°N, 18.2°E for Visby, 54.8°N, 17.2°E for Łeba, 46.2°N, 30.8°E for Odessa, 45.2°N, 33.2°E for Yevpatoriya and 45.2°N, 36.2°E for Kerch.

Also, four different atmospheric (circulation) indices were used in the analysis: (1) a station-based monthly NAO index (NAOi) obtained from the Climatic Research Unit of the University of East Anglia (http://www.cru.uea.ac.uk); (2) a principal-component based monthly NAO index (NAOcpc) (Thompson and Wallace 1998); (3) an AO index (AOi) obtained from the NOAA Climate Prediction Centre (ftp://ftp.cpc.ncep.noaa.gov/wd52dg and http://www.esrl.noaa.gov/psd/data/, respectively), and (4) a Siberian High index (SHi) calculated for January and February

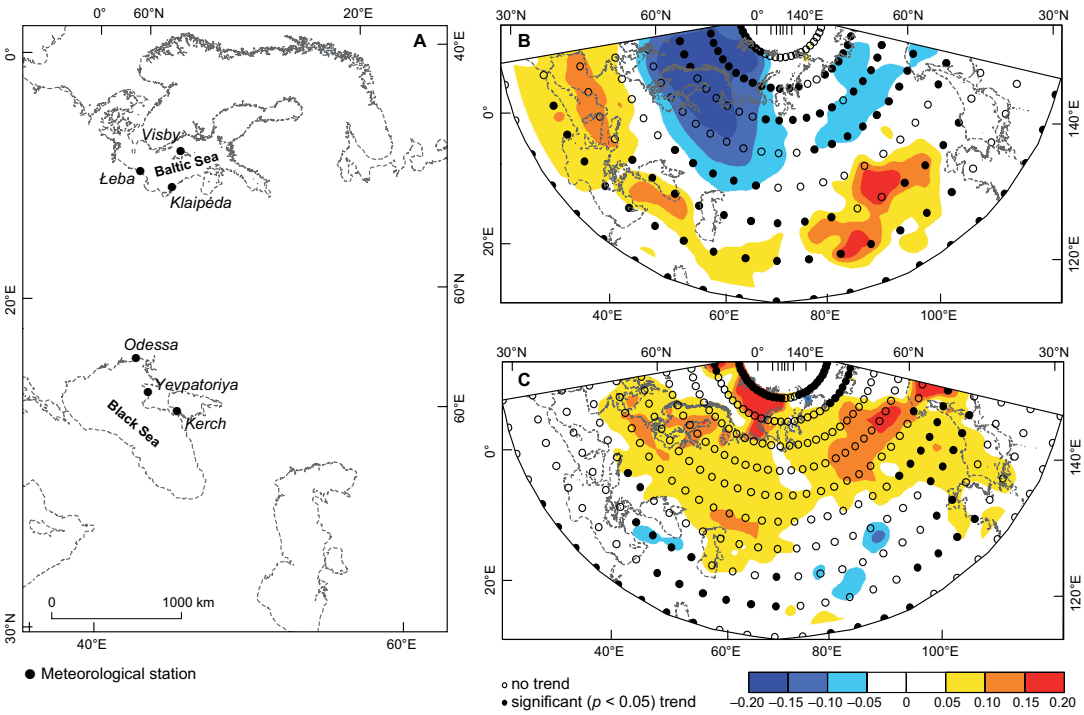

Fig. 1. (**A**) Locations of the meteorological stations, as well as (**B**) SLP, and (**C**) SAT trends (hPa/year and K/year, respectively) for the winter season (January–February) during 1950–2001. The colour scale indicates changes in hPa/year for SLP and K/year for SAT.

according to Panagiotopoulos *et al*. (2005). The first two indices (NAOi and NAOcpc) indicate intensity of the westerly flow over the north-east Atlantic and western Europe. The first is constructed using the difference the between sea-level air-pressure anomalies at two stations, one located in Iceland and the second on the Azores archipelago. The second index represents temporal coefficients of the leading mode of 700 mb height field in the northern hemisphere. Its spatial pattern is seasonally dependent. AOi is the index of the dominant pattern of non-seasonal sea-level air-pressure variations north of the 20°N latitude, and is characterized by air-pressure anomalies of one sign in the Arctic with the opposite anomalies at midlatitudes.

The sampled Eurasian SAT and SLP data were averaged for two consecutive months (January–February, March–April, …, November–December) for all months, starting from January. Further in the text these two.month periods will be referred to as "winter", "spring", "early summer", "summer", "autumn" and "pre-winter", respectively. These intervals represent the synoptic seasons' length better than the calendar seasons. Since individual synoptic seasons have different lengths in different years (Borisova and Rudicheva 1968, Girs and Kondratovich 1978), these averaged periods were chosen for the study because they maintain the month-to month identity within bi-monthly mathematical expectation or dispersion series (Polonsky and Basharin 2002). Also, pooling of two months' data into a single series was made in order to increase the series' length and increase the power of statistical analyses. However, this increase is expected to be marginal because of high temporal correlations between the merged months (Polonsky and Basharin 2002).

The dataset array was analyzed by singular value decomposition, or empirical orthogonal function (EOF) decomposition. This method is frequently used for data processing on a regular grid (Kim and Wu 1999).

According to this method, the original field $F(x,t)$ is expanded in series of certain functions $X_i(x)$ (spatial coefficient) with coefficients $T_i(t)$ (time coefficient) (i = 1, 2, 3, …) varying from one field to another. In this case, the procedure of determination of unknown functions is based on a single condition that the sum of squared errors of the expansion over all points of a given collection for the analyzed field must be minimum for all samples. Thus the empirical orthogonal functions minimizing the sum of squared errors of the expansion form the best possible basis for the representation of the original field.

In the present study, the traditional EOF method was used. Before applying this method to the meteorological fields, the linear trends were removed from the SLP and SAT fields. The presence of significant trends affects the space-time pattern of different modes if the trend is not removed before decomposition (Straus and Krishnamurthy 2007). The significance of the trend was tested using a non-parametric Mann-Kendall test (hereafter MK; Kendall 1975), which is adapted to climatic data analysis.

For the paired months, the EOF analysis includes only the first five spatial and temporal empirical modes of SAT and SLP whose contribution to the variance of the corresponding fields is maximal in Eurasia in 1950–2001. All other data (station data and indices) used in the study were de-trended and bimonthly averaged before the correlation with the leading SAT and SLP modes was tested. Pearson's correlations were considered significant at $p < 0.05$ and the trends when the absolute MK value was > 1.96. The length of the time series analysed here is constant (1950–2001, degrees of freedom = 50).

Results

Large scale SAT/SLP and regional temperature/precipitation trends

For several areas we found statistically significant SAT trends in the winter season: positive in the northernmost region (0.2 K/year, MK = 5.2) and East Asia, and negative in the Middle East (up to –0.07 K/year, MK = –3.8) (Fig. 1C). A similar spatial structure of winter linear trends is presented by Basharin (2009). That study analyzed a slightly larger domain and combined the data from two different reanalyzes (NCEP/NCAR and JMA). Also, negative SAT trends persisted over Scandinavia during the early summer and summer seasons (up to –0.06 K/year, MK = –4.7), and positive trends were found for the Baikal Lake–Mongolia region in summer (up to 0.1 K/year, MK = 3.6). In other seasons, SAT trends are lower in magnitude and statistically insignificant.

The most prominent SLP trends were also found for the winter seasons (Fig. 1B). The area of statistically significant negative trends covers northern Europe and the northern part of Asia, with maximal values over the Norwegian Sea (–0.2 hPa/year, MK = –2.7). An area with positive trends extends from Gibraltar to Mongolia, while statistically significant spots are surrounded only with –0.12 hPa/year isolines. The spatial structure of the trend areas (their distribution and values) as presented by Polonsky (2008) is very similar to our findings; however, in the present study, the negative SLP trends over northern Europe are insignificant (Fig. 1B). Winter SLP trends seem to be very consistent with the results concerning changes in atmospheric circulation during the last decades of the last century (Fyfe *et al*. 1999, Deser *et al*. 2000, Hilmer and Jung 2000, Thompson *et al*. 2000). The summer SLP trends have also a similar spatial structure (not shown): a no-trend area extends over northern Asia and eastern Siberia, and a significant and positive trend area over the Mongolia–Manchuria region (up to 0.13 hPa/year, MK = 5.5).

Statistically significant and positive trends in temperature series were detected only for the Baltic sub-region: Klaipėda in spring (0.05 K/year, MK = 3.4), Visby in spring (0.03 K/year, MK = 2.3), and Łeba in winter (0.12 K/year, MK = 3.2). A negative significant trend was found for Kerch in the pre-winter season (–0.04 K/year, MK = –2.6). Significant precipitation trends were found only for the northern Black Sea sub-region: Yevpatoriya negative in winter (–0.73 mm/year, MK = –2.8), and Kerch positive in spring (0.55 mm/year, MK = 2.2).

Eurasian SAT and SLP leading modes and their interlinks

Only the first five leading modes of SAT and SLP were analyzed in this study. Together they explain 57%–73% of the SAT and 67%–85% of the SLP data variance. We decided to analyze the first five modes because the following modes (6th, 7th, etc.) are capable of representing a very small part of dispersion of the considered fields, and each one explains no more than 3% of the variance. Conversely, the first two modes explain around 50% of data variance, with the highest contribution in the cold half of the year. The lowest percentage of the data variance explained by the first two modes for SAT occurs in early summer and summer and for SLP in the entire warm half of the year.

The first SAT mode in winter (28.8%) represents one central spatial pattern extending over most of northern Eurasia, with the highest spatial coefficients over northwestern Yakutya (Fig. 2A). The second and third modes show a bipolar structure between the Arctic and Siberia and between the Baltic–Scandinavian and western Siberia–central Asia regions (Fig. 2B and C). The second one clearly shows the structure of the Siberian High pattern (Fig. 2B) (Panagiotopoulos *et al*. 2005). The next winter modes (4th and 5th) show multiple-center patterns and reflect large-scale tropospheric wave structure (Fig. 2D and E). In particular, the fourth mode is the Scandinavian pattern with centers over Scandinavia and northeastern Europe. These are reminiscent of a wave train and have been linked to tropical convection via Rossby wave propagation (Seierstad *et al*. 2007). In its positive phase, it is often associated with a blocking high over Scandinavia. The storms, therefore, tend to propagate to the north and south of this anomaly.

The spring SAT modes seem to be very similar to the winter ones (Fig. 3A–E): the first mode is almost identical but with the opposite sign, the second is similar to the winter third mode. However, centers of both signs are shifted to the east by 20°–25°. The third spring mode is similar to the winter second mode. The fourth mode shows multiple-center structures, corresponding to wave number 2 of the pattern over Eurasia–North Atlantic. The large scale wave's structure is a dominant feature in the SAT spring modes. In summer (Fig. 4A–E), almost entire Eurasia is covered by negative spatial coefficients, except for Fenoscandia and the Barents Sea in the first SAT mode. This structure has three main centers in Asia: Taymyr, eastern Kazakhstan and Manchuria. However, for the analyzed sub-regions the most important are the second and third modes, which together explain 22% of the data variance. The spatial structure of these modes is distinctly meridional and one of the centers is located directly at (2nd mode) or close to (3rd mode) the analyzed sub-regions. In autumn (Fig. 5A–E), the first SAT mode has only one center over northern Siberia and monotonic structure across Eurasia, while the others have bi- or multiple-polar structures. The prewinter 2, 4 and 5 SAT patterns (Fig. 6A–E) have high identical structures, similar to the corresponding spring modes, while the first one is similar to the second winter pattern (Fig. 1A) associated with the structure of the Siberian High. The third prewinter SAT pattern is similar to the first winter one (Fig. 3A), i.e. NAO pattern. The distribution of spatial coefficients clearly reflects storm track positions from the North Atlantic to the Eurasian interior and has been seen in many types of data based on observation (Trigo 2005, Harnik and Chang 2002).

The spatial structure of the leading SLP mode (Figs. 2–7F) is better expressed in terms of the amplitude's strength of minimum/maximum centers than SAT pattern mode, particularly in winter. The bipolar structure of the first mode corresponds with Arctic oscillation patterns over Eurasia. The second mode has a dipolar structure: two poles of the same sign lie over northern Siberia and the Mediterranean, and the opposite one over Scandinavia. This mode resembles the East-Atlantic pattern (Fig. 2G) (except for the center over northern Siberia) and significantly correlates with the temporal variability of the East-Atlantic pattern (Barnston and Livezey 1987). The third mode represents a complex pattern with large areas of negative signs in Siberia and western Europe separated by a narrow zone of the opposite sign, which extends from its source over the Arctic (Fig. 2H). The structure of the springtime leading SLP modes (Fig. 3F–J) shows similarity to the winter modes. The first

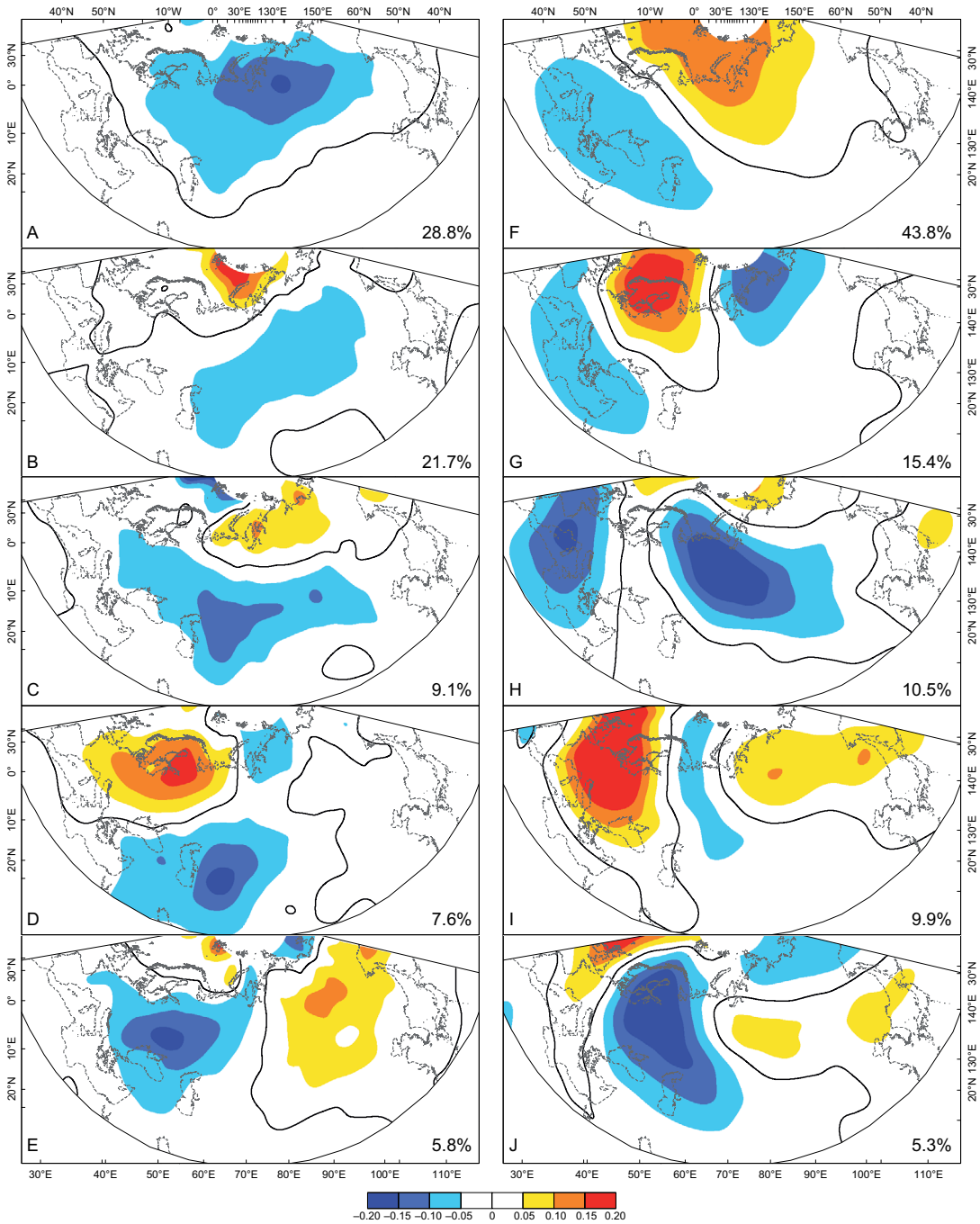

Fig. 2. The spatial patterns of the first five EOF modes of (**A**–**E**) surface air temperature and (**F**–**J**) sea-level air pressure for winter (January–February). Percentages of explained variance of the correspondent EOF mode are given in the lower right-hand-side corners. The colour scale indicates changes in °C for surface air temperature, and hPa for sea-level air pressure.

mode has one pole centered in the Arctic and includes vast territories to the south, from the British Isles to the Ochotsk Sea. The opposite pole is observed over the Mediterranean Sea.

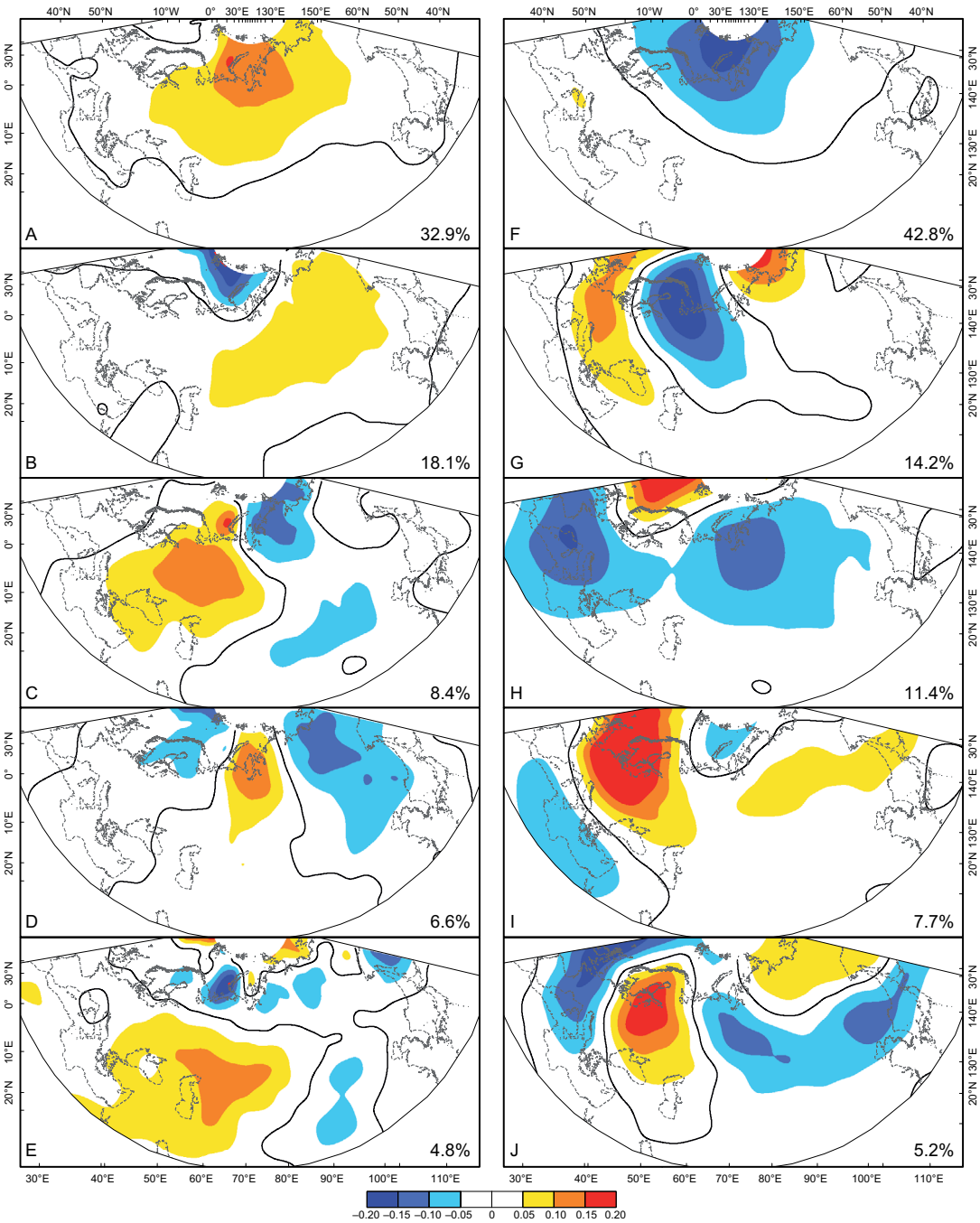

Fig. 3. The spatial patterns of the first five EOF modes of (**A**–**E**) surface air temperature and (**F**–**J**) sea-level air pressure for spring (March–April). Percentages of explained variance of the correspondent EOF mode are given in the lower right-hand-side corners. The colour scale indicates changes in °C for surface air temperature, and hPa for sea-level air pressure.

The second mode, as well as its winter counterpart, has an almost identical three-pole structure, however, shifted to the northeast. The first three early summer SLP modes (Fig. 3F–J) have more

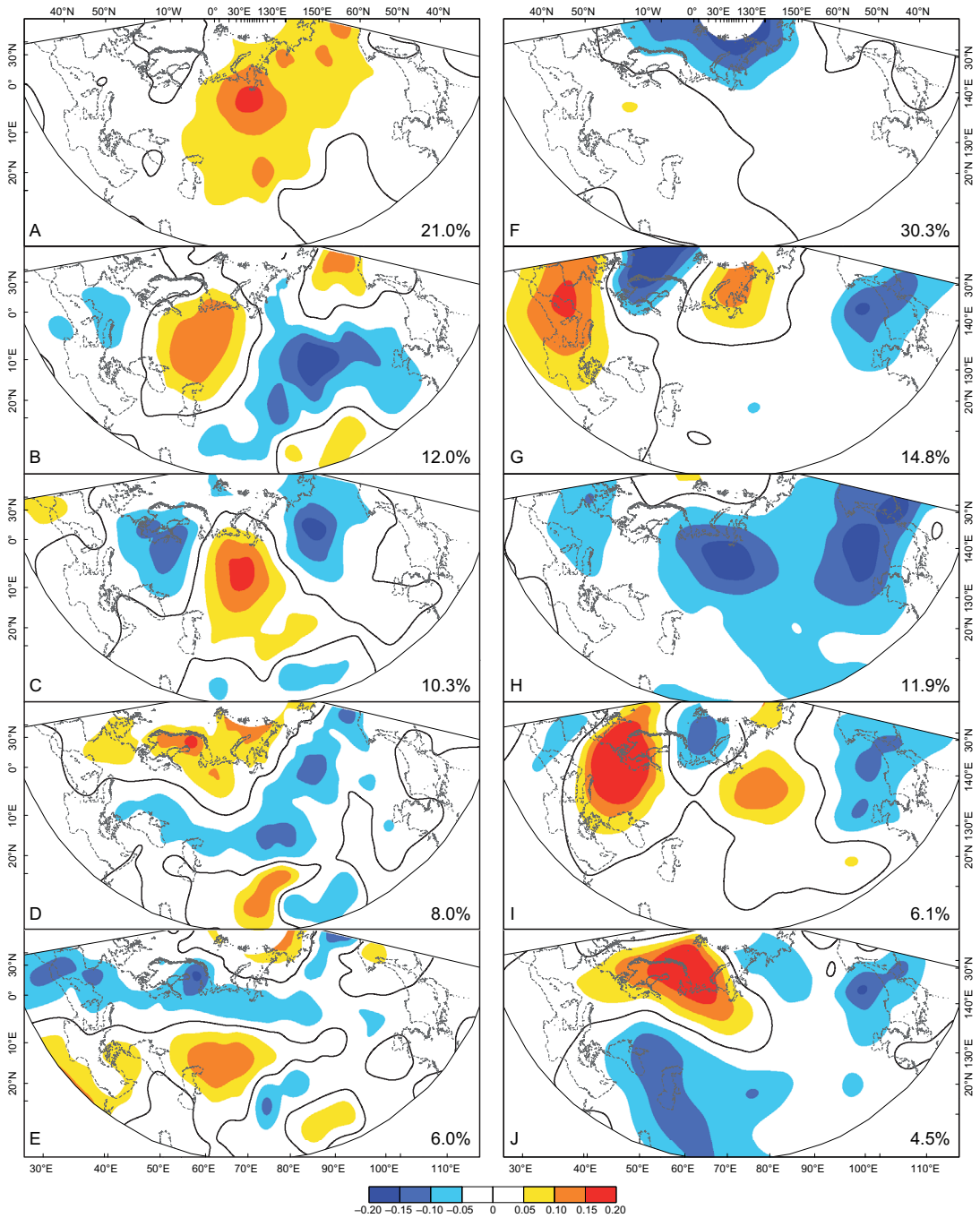

Fig. 4. The spatial patterns of the first five EOF modes of (**A**–**E**) surface air temperature and (**F**–**J**) sea-level air pressure for early summer (May–June). Percentages of explained variance of the correspondent EOF mode are given in the lower right-hand-side corners. The colour scale indicates changes in °C for surface air temperature, and hPa for sea-level air pressure.

or less monotonic structures because centers of action are less pronounced in extension and intensity in this season. The structure of the summer SLP modes (Fig. 4F–J) changes from

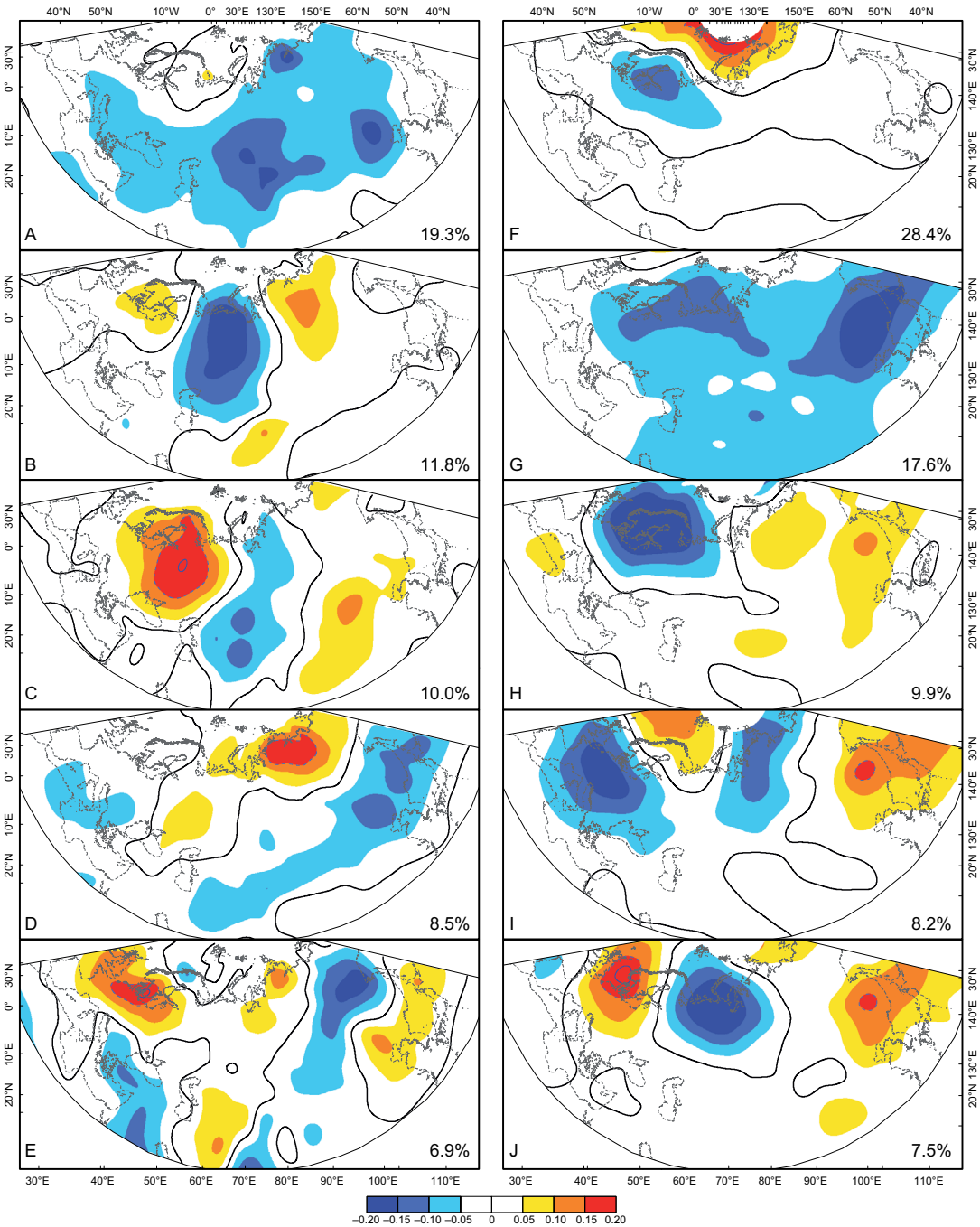

Fig. 5. The spatial patterns of the first five EOF modes of (**A–E**) surface air temperature and (**F–J**) sea-level air pressure for summer (July–August). Percentages of explained variance of the correspondent EOF mode are given in the lower right-hand-side corners. The colour scale indicates changes in °C for surface air temperature, and hPa for sea-level air pressure.

latitudinal bipolar in the first mode to multiple centers of the same sign in the second one, and multipolar in the third. Autumn SLP modes (Fig. 5F–J) show increased large-scale tropo-

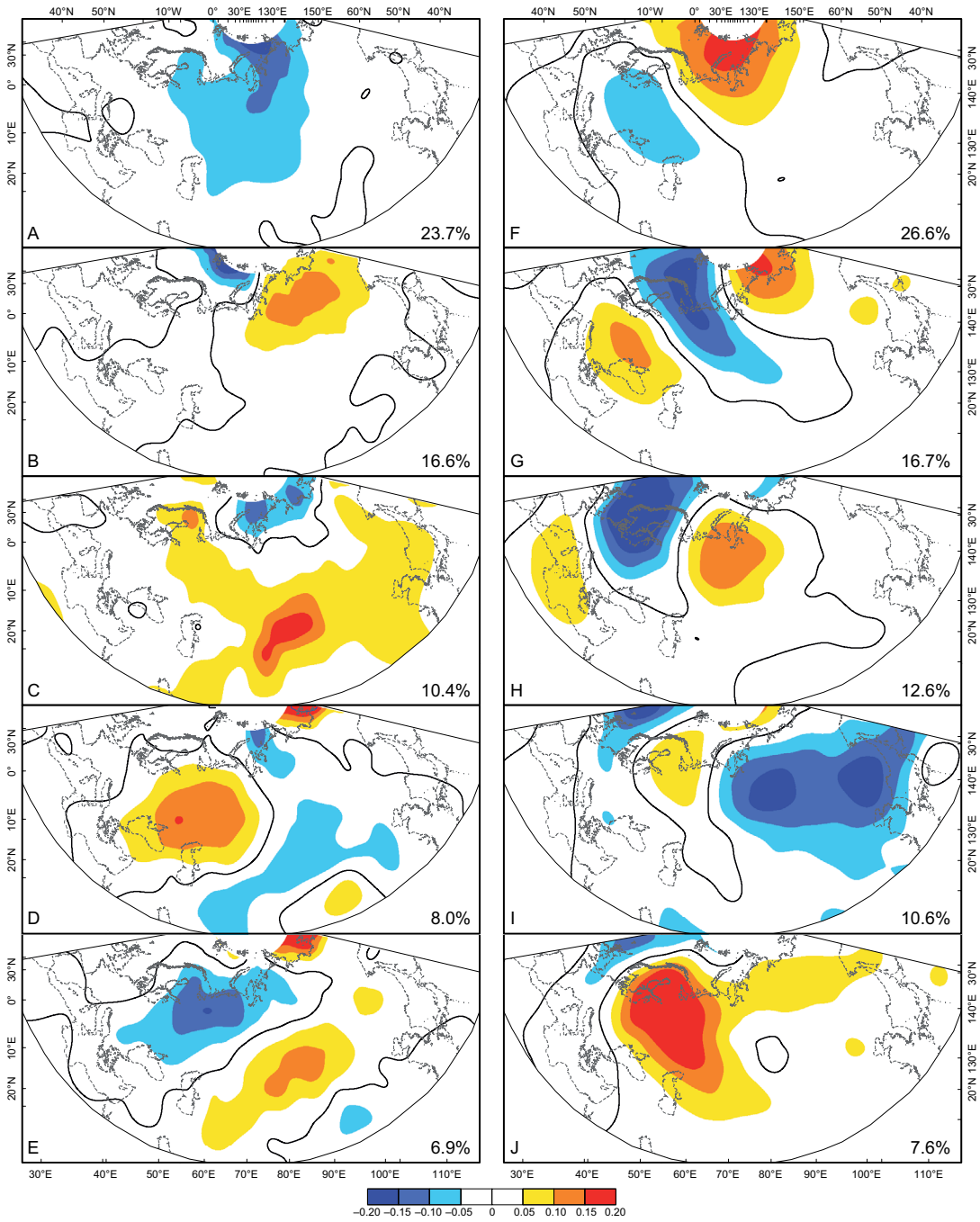

Fig. 6. The spatial patterns of the first five EOF modes of (**A**–**E**) surface air temperature and (**F**–**J**) sea-level air pressure for autumn (September–October). Percentages of explained variance of the correspondent EOF mode are given in the lower right-hand-side corners. The colour scale indicates changes in °C for surface air temperature, and hPa for sea-level air pressure.

spheric wave activity, the first two have a sub-zonal spatial structure, while the remaining three are strictly meridional. The first pre-winter SLP mode is similar to its autumn counterpart, but

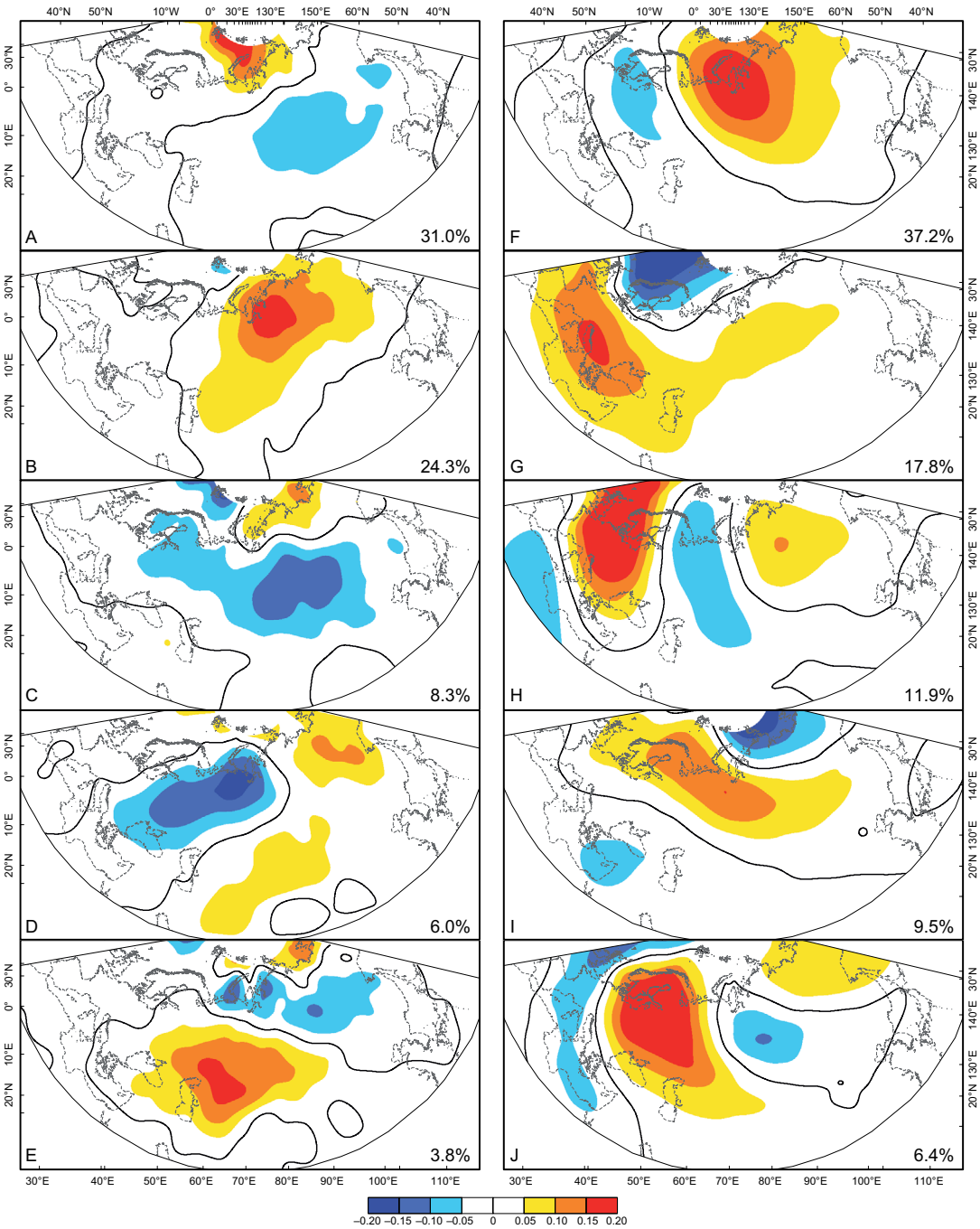

Fig. 7. The spatial patterns of the first five EOF modes of (**A**–**E**) surface air temperature and (**F**–**J**) sea-level air pressure for pre-winter (November–December). Percentages of explained variance of the correspondent EOF mode are given in the lower right-hand-side corners. The colour scale indicates changes in °C for surface air temperature, and hPa for sea-level air pressure.

the northern pole is shifted to the southeast, the second mode exhibits zonal flow *versus* a blocking structure over large parts of Europe, and the third mode's structure is strictly meridional with

a greatly enhanced pole over the North Sea (Fig. 6F–J). The course of the temporal coefficient' distribution of the first winter SLP mode (43.8%) has quite a similar shape as its SAT counterpart.

Analyzing the temporal variability of the patterns discussed above, we found that the strong correlation between corresponding modes of air pressure and temperature is detected only in the winter season ($r_p = 0.72, p < 0.01$; $r_p = 0.62, p < 0.01$; $r_p = 0.52, p < 0.01$; $r_p = 0.49, p < 0.01$; and $r_p = 0.45, p < 0.01$; respectively for all five leading SAT and SLP modes). That points to a strong ocean–atmosphere–land interaction, particularly in winter. Therefore, these winter patterns (SAT and SLP) manifest themselves over Eurasia as a dynamically compatible phenomenon in terms of temporal coherence behavior. In other seasons, there was no coherence in their relationships. In the spring, the relationships are weaker: the first SLP mode shows strong correlations with the first two SAT modes, while the fourth SAT mode correlates with 2–4 SLP modes. Interrelationship between SAT and SLP modes during early summer and summer is very weak, except for the third modes in early summer. In autumn correlation links become stronger again. Statistically significant coefficients ($r_p \le 0.52, p < 0.01$) were found for the first, second and fourth modes. In addition, the first SLP mode correlates with the second SAT mode. The pre-winter season was also quite similar to autumn. Strong correlations ($r_p \le 0.66, p < 0.01$) were detected between the first and third modes and between the first SLP mode and the second SAT mode. The persistence of the large scale surface temperature and air-pressure fields showed the complex nature of their inter-seasonal variability.

Coherence between SAT/SLP modes and different indices (NAOi, NAOcpc, AOi and SHi) were also studied. Having analyzed the SLP field, it is worth noting that SHi is a product of a sea-level air-pressure field over large areas in the interior of Asia; therefore, it has good coherence, not only with the leading hemispheric oscillation (correlation with AO is –0.46) but also with the analyzed Eurasian SLP modes. Statistically significant winter-season correlations ($r_p \le 0.60, p < 0.01$) between AOi and the first, second, third and fourth modes' temporal coefficients were found. The correlations between the first SLP mode and the NAOi, NAOcpc and AOi indices appeared to be the best for this season ($r_p \le 0.88, p < 0.01$); however, the second mode also has statistically significant correlations with those indices ($r_p \le 0.56, p < 0.01$). The similar strength of correlations was also found for early summer (with approximately the same magnitude), while for summer the best correlations were calculated for the third mode ($r_p \le 0.47, p < 0.01$). In other seasons, the first SLP leading mode correlate better with AOi or NAOcpc than with NAOi, except for the pre-winter season, when the second mode has the best correlation ($r_p = 0.81, p < 0.01$).

For the SAT field, all three indices (NAOi, NAOcpc and AOi) contribute almost equally. The first and third SAT modes correlate significantly ($r_p \le 0.63, p = 0.05$ and $r_p \le 0.55, p < 0.01$, respectively) with the three above-mentioned indices in winter–spring seasons. In other seasons, significant correlations with these SAT modes are also found, but the correlation coefficients are low ($r_p = 0.29–0.38, p = 0.04–0.005$).

The relationship between atmospheric circulation indices and regional temperature/precipitation

Leading winter and spring SAT modes correlate significantly with the corresponding regional Baltic temperatures, with the best corralation found for Visby and the fourth mode in winter (Table 1). In the Black Sea region, only springtime temperatures and the SAT first mode were correlated. In winter, the strongest correlations were found with the fifth and third modes, which together account for almost 15% of the seasonal data variation. It is worth noting that the winter temperature at the Kerch station shows a reliable statistical relationship with almost all analyzed SAT modes except for the fourth. In early summer, no significant correlations were found with the two first leading modes, however, strong correlations in both regions were detected with the third mode: higher coefficients for the Baltic stations (Klaipėda: $r_p = –0.70, p < 0.001$), and weaker for the Black Sea stations. In summer, the temperatures in both regions also correlate well with the third mode. However, the Black

Sea stations also show a reliable relationship with the first mode and the Baltic stations with the second one (except Łeba). The analysis showed that in the autumn and pre-winter seasons the correlations between station temperatures and SAT temporal coefficients are the weakest. The autumn temperature at two Baltic stations correlates with the first mode (Table 1) and the Black Sea station temperature with the fourth and fifth modes. There is no correlation between regional temperatures and the first two leading modes in the pre-winter season. The temperatures at the Baltic stations correlate only with the third mode (negative coefficients) and the temperatures at the Black Sea stations with the fourth one.

The correlations between regional precipitation and SAT modes are weak. There are no strong correlations between the Baltic and Black sea regional precipitation and the first three leading SAT modes in all seasons. However, there are exceptions: Klaipėda station in winter (the first mode) and Klaipėda and Łeba in summer (2nd mode). The weakest correlation between precipitation and SAT modes in the Black sea region was found for the Yevpatoriya station.

The leading SLP modes appeared to correlate better with regional temperatures than their SAT counterparts in winter and spring. Baltic temperatures correlate strongly with the first two modes in winter (inverse relationship) and the first mode in spring, while in the Black Sea region statistically significant correlations with the winter first three modes and first two in spring were found only for the Odessa station (Table 1). Precipitation at the other two stations correlates significantly with the third winter and the second spring mode. In early summer, there are the weakest correlations between SLP modes and regional temperatures, except for the first mode at the Visby station (r_P = 0.34, p = 0.013). In summer, stronger correlations were detected for the Black Sea than for the Baltic regions: negative correlations with the first mode are found for Klaipėda and Visby, and with the second mode for the Black Sea stations. Moreover, at the Odessa station temperatures in summer

Table 1. Seasonal Pearsons's correlations (r_P) between the first five EOF modes of SAT/SLP and sub-regions' temperature (Temp.) and precipitation (Prec.). Significant correlations (at $p < 0.05$) are set in boldface.

Season	SAT/SLP mode		Stations											
			Klaipėda		Visby		Łeba		Odessa		Yevpatoriya		Kerch	
			SAT	SLP	SAT	SLP	SAT	SLP	SAT	SLP	SAT	SLP	SAT	SLP
Jan–Feb (winter)	1	Temp.	**–0.55**	**–0.63**	**–0.58**	**–0.69**	**–0.41**	**–0.53**	**–0.31**	**–0.30**	–0.24	–0.13	**–0.29**	–0.16
		Prec.	**–0.44**	–0.25	0.02	0.10	–0.24	–0.14	0.23	**0.40**	0.17	0.13	–0.10	0.03
	2	Temp.	0.02	**–0.48**	0.07	**–0.46**	0.02	**–0.46**	–0.17	**–0.40**	–0.24	–0.27	–0.27	–0.22
		Prec.	0.03	**–0.39**	0.05	–0.23	–0.08	–0.19	–0.06	0.17	**–0.32**	**0.30**	**–0.39**	**0.31**
	3	Temp.	–0.23	0.13	–0.18	0.02	–0.24	0.06	**–0.32**	**0.43**	**–0.30**	**0.49**	**–0.29**	**0.44**
		Prec.	**–0.45**	0.22	**–0.34**	0.10	–0.25	0.21	0.25	–0.06	–0.21	**0.42**	–0.20	**0.41**
	4	Temp.	**0.59**	–0.04	**0.65**	0.01	**0.64**	–0.12	0.24	–0.04	–0.06	0.07	–0.11	0.10
		Prec.	–0.09	**0.37**	–0.18	0.08	–0.21	0.23	**–0.59**	0.27	**–0.44**	**0.29**	**–0.49**	**0.33**
	5	Temp.	**–0.36**	0.04	–0.18	–0.01	**–0.34**	0.08	**–0.72**	**0.38**	**–0.75**	**0.49**	**–0.70**	**0.49**
		Prec.	–0.14	0.15	0.09	0.19	–0.03	0.21	–0.24	**0.37**	–0.18	0.19	0.06	0.00
Mar–Apr (spring)	1	Temp.	**0.61**	**0.58**	**0.64**	**0.65**	**0.44**	**0.52**	**0.47**	**0.41**	**0.37**	0.27	**0.32**	0.21
		Prec.	0.07	0.05	0.03	–0.04	0.05	0.00	–0.16	–0.22	–0.06	–0.10	–0.18	–0.27
	2	Temp.	0.24	0.12	0.27	0.11	**0.42**	0.07	0.17	**0.51**	0.12	**0.48**	0.10	**0.45**
		Prec.	0.01	**0.56**	–0.10	**0.51**	0.01	**0.57**	–0.05	0.10	0.02	0.15	–0.14	0.10
	3	Temp.	0.17	–0.01	0.08	–0.04	0.10	0.21	0.23	0.17	**0.35**	0.19	**0.33**	0.20
		Prec.	0.22	–0.03	0.23	0.00	0.18	0.08	0.00	0.23	–0.13	0.25	–0.17	0.23
	4	Temp.	0.24	0.12	0.27	0.11	**0.42**	0.07	0.17	**0.51**	0.12	**0.48**	0.10	**0.45**
		Prec.	0.14	–0.27	0.08	–0.17	0.21	–0.06	**0.46**	0.24	**0.54**	0.12	**0.35**	0.12
	5	Temp.	–0.06	–0.06	–0.15	0.05	0.05	–0.04	0.24	–0.12	0.26	–0.23	0.27	–0.19
		Prec.	**0.28**	–0.20	**0.33**	**–0.33**	0.21	**–0.33**	0.17	0.14	0.24	0.21	0.17	0.27

continued

Table 1. Continued.

Season	SAT/SLP mode		Stations											
			Klaipėda		Visby		Łeba		Odessa		Yevpatoriya		Kerch	
			SAT	SLP	SAT	SLP	SAT	SLP	SAT	SLP	SAT	SLP	SAT	SLP
May–Jun	1	Temp.	–0.05	0.17	–0.04	**0.34**	–0.14	0.24	–0.03	–0.05	–0.09	–0.18	–0.01	–0.18
(early		Prec.	0.00	–0.25	0.07	**–0.29**	0.07	–0.13	–0.02	–0.02	0.08	0.21	0.07	**0.36**
summer)	2	Temp.	0.26	0.13	0.10	0.22	0.06	0.15	0.05	0.04	0.11	0.10	0.24	0.04
		Prec.	0.11	0.04	0.09	–0.05	–0.04	0.09	–0.13	0.06	0.12	0.17	0.01	0.12
	3	Temp.	**–0.70**	–0.24	**–0.65**	–0.18	**–0.37**	–0.19	**–0.39**	–0.07	**–0.31**	–0.03	**–0.36**	–0.03
		Prec.	0.21	0.06	**0.35**	–0.01	0.26	0.18	–0.01	–0.04	–0.06	–0.20	0.21	–0.02
	4	Temp.	0.26	0.06	**0.29**	–0.08	–0.06	–0.17	–0.07	0.07	–0.06	0.09	–0.09	0.19
		Prec.	0.02	–0.07	–0.01	0.09	–0.02	0.01	0.10	–0.09	0.13	0.11	**0.37**	0.26
	5	Temp.	–0.25	**0.35**	**–0.44**	0.27	**–0.36**	–0.06	–0.10	0.02	–0.03	0.08	–0.04	0.09
		Prec.	0.05	–0.15	0.18	–0.21	0.05	–0.14	0.03	–0.03	–0.06	0.03	–0.18	0.00
Jul–Aug	1	Temp.	–0.09	**–0.43**	–0.05	**–0.47**	0.16	–0.25	**–0.33**	–0.20	**–0.33**	–0.05	**–0.28**	–0.08
(summer)		Prec.	0.23	**0.53**	0.19	**0.32**	0.10	**0.61**	0.27	0.01	0.16	–0.20	0.00	–0.20
	2	Temp.	**0.30**	0.06	**0.40**	–0.11	0.16	–0.03	–0.13	**0.33**	–0.18	**0.28**	–0.23	**0.32**
		Prec.	**–0.40**	0.02	–0.22	0.09	**–0.30**	0.20	0.01	–0.11	0.14	–0.16	0.08	–0.11
	3	Temp.	**0.75**	0.00	**0.57**	–0.13	**0.40**	–0.12	**0.61**	**0.28**	**0.45**	0.19	**0.53**	0.12
		Prec.	–0.02	0.16	0.03	0.19	–0.10	0.18	0.08	–0.20	0.05	**–0.34**	0.12	–0.12
	4	Temp.	–0.07	–0.11	–0.02	–0.10	0.08	**–0.29**	–0.03	**–0.28**	0.04	–0.24	0.13	**–0.32**
		Prec.	0.25	–0.12	–0.01	0.06	0.11	0.07	–0.10	0.07	–0.09	0.16	–0.22	0.10
	5	Temp.	**0.39**	**–0.53**	**0.51**	**–0.46**	**0.29**	**–0.33**	0.06	–0.26	–0.07	–0.15	–0.12	–0.18
		Prec.	**–0.38**	0.03	**–0.31**	–0.12	**–0.54**	0.00	–0.02	–0.22	0.11	–0.07	0.22	–0.12
Sep–Oct	1	Temp.	**–0.45**	**–0.35**	**–0.41**	–0.23	–0.26	–0.10	–0.04	0.03	–0.07	0.05	–0.15	0.05
(autumn)		Prec.	–0.24	0.23	0.02	0.26	–0.21	0.13	0.09	0.06	0.07	0.21	0.17	0.06
	2	Temp.	0.08	0.24	0.15	–0.04	–0.06	0.12	–0.13	0.03	–0.08	–0.10	–0.19	0.07
		Prec.	–0.17	**0.44**	–0.11	0.16	0.04	0.25	–0.05	–0.15	–0.07	0.08	0.01	–0.12
	3	Temp.	–0.16	**0.56**	–0.14	**0.57**	–0.02	**0.44**	–0.05	**0.28**	0.01	0.17	–0.03	0.22
		Prec.	0.02	–0.01	0.07	0.04	0.06	–0.05	–0.07	–0.01	–0.07	–0.11	0.02	–0.17
	4	Temp.	0.14	0.08	0.18	0.13	0.19	0.04	**0.50**	**–0.37**	**0.58**	**–0.45**	**0.65**	**–0.42**
		Prec.	**0.30**	**–0.41**	**0.28**	–0.21	**0.35**	**–0.37**	0.16	0.04	0.04	0.06	0.04	0.12
	5	Temp.	**–0.36**	–0.16	–0.21	–0.01	**–0.29**	–0.02	**–0.39**	**–0.55**	**–0.37**	**–0.53**	**–0.33**	**–0.47**
		Prec.	–0.18	**–0.38**	–0.15	**–0.49**	–0.11	**–0.39**	0.18	0.12	0.09	0.17	0.10	0.06
Nov–Dec	1	Temp.	–0.02	–0.22	0.11	–0.10	0.11	0.02	0.11	0.11	0.07	0.19	0.00	0.12
(pre-winter)		Prec.	–0.03	–0.09	0.23	**0.40**	–0.03	–0.10	0.15	**0.31**	–0.09	0.04	**–0.33**	–0.19
	2	Temp.	–0.03	0.13	–0.17	**0.36**	–0.13	**0.33**	–0.11	–0.04	–0.08	–0.21	–0.03	–0.25
		Prec.	0.25	–0.04	–0.21	–0.13	0.23	–0.05	–0.10	–0.14	0.08	**–0.31**	0.18	–0.22
	3	Temp.	**–0.42**	–0.11	**–0.44**	**–0.34**	**–0.34**	**–0.30**	–0.18	0.16	0.05	**0.34**	0.07	**0.34**
		Prec.	–0.02	**0.37**	0.04	0.26	0.13	**0.41**	**0.41**	**0.29**	0.27	0.19	0.14	0.24
	4	Temp.	–0.27	**–0.45**	–0.10	–0.24	0.02	–0.21	**–0.61**	–0.20	**–0.55**	–0.15	**–0.52**	–0.13
		Prec.	**–0.39**	–0.16	**–0.41**	–0.24	**–0.36**	–0.18	–0.21	0.20	–0.04	0.22	–0.03	0.05
	5	Temp.	0.11	**–0.28**	–0.09	–0.18	–0.14	–0.14	0.25	**–0.67**	**0.43**	**–0.65**	**0.46**	**–0.58**
		Prec.	0.09	**–0.33**	0.18	**–0.38**	0.21	**–0.31**	0.20	**–0.29**	0.07	–0.05	–0.06	0.11

correlated with second to fourth SLP modes (Table 1). Autumn and pre-winter leading SLP modes correlate better with the Baltic temperatures. Strong correlations with the autumn third mode was found for all three Baltic stations, and with the first one only for Klaipėda. The correlations in the Black Sea region exist only between the temperature in Odessa and the third SLP mode. However, very strong negative correlations with the fourth and fifth modes were found for all three stations. In the pre-winter season, significant correlations with the second and third modes were found only for Visby and Łeba; the latter mode also correlates with temperatures at

Yevpatoriya and Kerch.

A completely different picture is seen when analyzing relationships between SLP modes and regional precipitation (Table 1). All analyzed winter SLP modes correlate significantly with Black Sea precipitation: at Odessa with the first and fifth modes, at other stations with second–fourth modes. In the Baltic region, only Klaipėda precipitation correlates with the second and fourth modes. Black Sea regional precipitation does not correlate with the SLP modes in spring to autumn (except Kerch in early summer), while for the Baltic stations, strong correlations with the spring second mode (positive) and summer first mode (positive) were found. Additionally, precipitation at Visby correlates with the early-summer first mode, and precipitation at Klaipėda with the autumn second mode. In the pre-winter season, the third and fifth modes correlate with precipitation at the Baltic stations and Odessa, respectively.

However, taking into consideration all the significant correlations, it is essential to remember the relative importance of the spatial distribution's amplitude of SLP/SAT large-scale EOF patterns. The real signal of the reconstructed field is a product of multiplying the temporal coefficient by its spatial distribution's amplitude, presented by the large-scale EOF pattern. Thus, the amplitude of the pattern plays an important role in terms of the local and regional climate formation.

Discussion

The 2nd half of the 20th century was characterized by a positive temperature trend around the globe and a negative sea-level air-pressure trend in the polar regions; however, smaller-scale trend analysis shows large diversity, both on spatial and temporal scales. Even in winter, when temperature trends have the largest magnitude, significant trends are found only for about 25% of the analyzed area and only in very specific locations, such as the northeastern Atlantic, part of Scandinavia and part of the Middle and Far East. In summer, areas with significant trends are smaller than in winter. The defined sea-level air-pressure trends match the trends found for the Arctic in the last two decades of the 20th century (IPCC 2007). Winter air-pressure tends decrease in northern Europe and the northernmost Asia, and increase in the latitudinal belt southwards. This is also reflected in significant trends of circulation indices: NAO/AO-like indices show increasing trends in winter while the Siberian High maximum decreases. The results agree with previous studies concluding that Eurasian trends are the outcome of the storm track changes driven by the inter-decadal behavior of the NAO-like meridional dipole pattern in the North Atlantic. Local-scale trends display much higher spatial variability. A positive winter-temperature trend was found for only one station in the Baltic region, while in spring a positive trend was found for the other two Baltic-region stations. No significant precipitation trends were found. Precipitation tends to decrease in winter and spring in the Black Sea region and only locally.

These trends could be induced by different factors. Some researchers consider them a manifestation of anthropogenic activity, while others argue that half-century-long trends are a part of much longer climate fluctuations (Polonsky 2008). Moreover, some scientists claim that trends are a clear demonstration of the inter-decadal atmospheric circulation variability and related changes in intensity and the spatial shift of the centers of action and storm tracks (Savelieva *et al*. 2004, IPCC 2007). On the other hand, significant changes in the NAO-like circulation in seasonal storm track position and in large-scale heat and moisture transport may partly be caused by anthropogenic processes (Stephenson *et al*. 2006). Consequently, the analysis of time series of selected atmospheric-circulation indices also reveals significant trends. NAO-like indices and SHi in winter show opposite trends. That goes along with the inter-decadal NAO tendency to positive values (they tend to remain in one extreme phase) and accounts for a substantial part of the observed wintertime surface warming over not only Europe but also the Siberian region. Generally, the circulation changes in the winter season have been already well documented in the scientific literature, while other seasons received much less attention (Panagiotopoulos *et al*. 2005). Here, all sea-

sons were taken into consideration. Moreover, abrupt atmospheric circulation changes in the cold period between the 1970s and 1980s have been suggested to result in trend enhancement (Brönnimann *et al*. 2009, Jacobeit *et al*. 2009).

The most prominent modes of surface air temperature (SAT) show continental scale patterns (*see* Fig. 2A and B), with their center located over northern Asia. Such a structure of leading modes is typical for almost all seasons of the year, while in early summer and summer there are scattered centers reflecting the complexity of processes inducing large scale thermal anomalies. SAT and SLP leading modes in winter show clear interlinks between their temporal coefficients. So they may be called dynamically compatible in terms of temporal coherence behavior. In other seasons there is no such coherence because SLP leading modes, in contrast to SAT counterparts, usually have a bipolar spatial structure reflecting the oscillatory nature of air-pressure fields, particularly over Europe. Other leading modes in all seasons show multiple-center patterns related to smaller-scale wave activity. Lower-order modes have a rather meridional spatial structure, indicating surface air-pressure dependence on the large tropospheric wave location and amplitude.

The examination of the lagged relationship between the consecutive seasons revealed existing inertia during the first half of the year (Figs. 2A, F and 3A, F). Strong correlations were found between first SAT leading modes in consecutive seasons: the modulus of correlation coefficients gradually increases from winter to summer and then drops below significance level in autumn and pre-winter. Conversely, month-to-month variability of the leading SLP modes shows almost no inertia in the warm season. However, there are strong correlations between consecutive seasons starting from autumn. This clearly indicates that the structure of the leading SAT modes depends on the gradually retreating permanent snow cover in spring over a vast territory, and on uniform heating in summer, while the structure of the leading SLP modes points to the rapidly increasing air-pressure gradients at middle and high latitudes.

A more explicit way of assessing how much variability in extracted temporal coefficients of SAT and SLP modes is explained by the different predictors (atmospheric circulation indices) is to examine correlations between different circulation indices. All indices used in this study are inter-correlated: many correlations are significant (at $p < 0.05$) in the cold half-year (winter and pre-winter seasons). However, in the warm half-year, correlations become weaker and are the weakest in summer between NAOi, and NAOcpc/AOi. In winter (January–February), all correlations between SHi and other indices are negative, which indicates strong coupling between the intensity of large scale circulation over the North Atlantic/Arctic sector and the cold core continental anticyclone.

The NAO-like meridional dipole pattern in the Atlantic may influence not only the first, but also the second or third large-scale EOF patterns; this agrees with the results presented by Slonsky and Yiou (2002). The NAO signal may be distributed among several EOF patterns using traditional EOF analysis. For example, in winter, two first modes associate with NAO-like large-scale EOF pattern. However, the relative importance of the spatial distribution's amplitude of the second SLP large-scale EOF pattern for the Baltic region has to be taken into account: the amplitude is far from zero in the second pattern (Fig. 2B), and close to zero in the first (Fig. 2A). Thereby, it is possible to find the real driving large scale pattern for the sub-region.

In general, many outlined relations between the SAT modes and different indices show a substantial circumpolar vortex impact on Eurasian temperatures in the first case, and a relationship between zonal circulation intensity and warm advection over Baltic–northwest Russia in the second one, whereas SHi correlates significantly with all analyzed winter SAT modes except for the first. This means that more than 44% of the variation in the SAT data over Eurasia in winter is related to the SH intensity variation. At the same time, AOi correlates with every season's first SLP modes. This can be explained by the fact that the loading pattern of AO is defined as the first leading mode from the EOF analysis of monthly mean height anomalies at the 1000 hPa level.

All circulation indices used in the study are bound up with the large-scale air-pressure field

structures and their temporal variability. However, processes they may represent are quite different: some are dynamically others, mostly thermally induced. If some of these indices were used in a model to predict one dependent variable (e.g. local temperature and/or precipitation or even SAT/SLP mode) and they were mutually correlated, such phenomenon would be called multicollinearity of predictors and would reduce reliability of modeling results. Therefore in this study, relationships between SAT/SLP modes and atmospheric circulation indices were analyzed separately for every index.

The Baltic regional temperatures are closely related to the patterns of the leading SAT modes in winter and spring, and the best correlations were found for the Visby station (Table 1). Form the Black Sea region, correlation exist only in spring. However, the Kerch station temperature is correlated with almost all analyzed winter SAT modes. In other seasons, correlations appear to be weaker with leading modes, except in summer for the Black Sea region. The winter and spring leading SLP modes correlate stronger with regional temperatures than with the SAT modes, and it only confirms the importance of atmospheric circulation in the cold season in the formation of temperature anomalies, particularly over the Baltic region. However, in the pre-winter season and for both regions there are no significant correlations with the leading modes. In summer, the Black Sea regional temperatures correlate with SLP better than do the Baltic ones. However, there is a large variability in correlation coefficients between stations. Thus, temperature variability in the Baltic Sea sub-region seems to be a part of continental-scale temperature anomalies that are induced by a different NAO/AO phase circulation in winter and spring, and depends on tropospheric large-scale wave positioning and amplitude in summer. Black Sea sub-region temperature anomalies are smallest in summer and show strong coupling with the high air-pressure system intensity and position over the Mediterranean.

Winter precipitation correlates better with the leading SLP modes in the Black Sea region (Table 1). However, in the other seasons correlations are very weak. Conversely, summer Baltic precipitation shows correlates with the first SLP mode, indicating cyclonic circulation with atmospheric fronts as the main contributors in this region, even in summer. Thus, in these seasons SLP modes better represent large-scale structure of migratory and stationary weather systems than SAT one in analyzed sub-regions.

The current study analyzed local-scale climate variability in the sub-regions by examining large scale surface temperature and air-pressure structures of Eurasia. It reveals the complex nature of their interrelationship. However, the results show that there are no sufficiently strong linear ties (being suitable for the statistical prediction purpose) between particular bi-monthly SAT/SLP patterns (also for station based circulation indices) and local-scale climate variability. It is likely that nonlinear methods are needed to establish such relations and analyze the local scale climate variability. They may improve the predictability on seasonal to interannual scales which still remains an important challenge for the future.

Conclusions

1. SAT and SLP trends in Eurasia in the second half 20th century show already well documented global-scale changes: strong positive temperature (SAT) and negative sea-level air-pressure (SLP) trends in the Eurasian polar region in winter, while positive SLP trends have an almost annular structure in the northern part of Eurasia. In the sub-regions, trends show no spatial uniformity, probably because of the high local climate variability/topographic influence.
2. On interannual-to-decadal time scales, a significant synchronous correlation between accordant modes of SAT and SLP EOF patterns is found. This fact suggests that there is a strong and stable Eurasian interrelationship between SAT and SLP large-scale fields, which results in the local climate of two sub-regions: the Black and Baltic Seas.
3. The NAO signal may be distributed among several EOF patterns using a traditional EOF analysis. When analyzing their influence on sub-regions, the relative importance of the local amplitude of the large-scale EOF pat-

terns in the sub-region of interest must be taken into account.

4. The Baltic Sea region is influenced by the patterns arising from (1) the NAO-like meridional dipole, and (2) from the Scandinavian patterns. While the second EOF mode (East Atlantic-like) and a large-scale tropospheric wave structure seem to be the main contributors to the Black Sea's SAT/SLP variability, the NAO-like meridional dipole pattern plays only a secondary role.
5. On a sub-regional scale, the SLP modes are a better "indicator" of local precipitation than SAT. Even in summer, the SLP modes represent cyclonic circulation patterns with atmospheric front activity which seems to be the main contributor to the local precipitation variability.

Acknowledgments: Much of the work of this paper was performed within the framework under the Ukrainian–Lithuanian cooperation joint project and the mobility grant TAP-19 of the Research Council of Lithuania. Also, part of this work was performed within the framework of the Associateship Scheme of the Abdus Salam International Centre for Theoretical Physics. The authors thank the joint projects for providing support. The study was also partly supported by the BSR Interreg IVB Project "Climate Change: Impacts, Costs and Adaptation in the Baltic Sea Region (BaltCICA). We are grateful to the reviewers for the constructive and helpful criticism of the first version of this paper.

References

Barnston A.G. & Livezey R.F. 1987. Classification, seasonality and persistence of low frequency atmospheric circulation patterns. *Mon. Wea. Rev.* 115: 1083–1126.

Basharin D.V. 2009. *Variability of the surface meteorological fields over Eurasia for the recent 30 years*. Preprint IC2009077, International Center Theoretical Physics, available at http://users.ictp.it/~pub_off/preprints-sources/2009/IC2009077P.pdf.

Beranová R. & Huth R. 2008. Time variations of the effects of circulation variability modes on European temperature and precipitation in winter. *Int. J. Climatol.* 28: 139–158.

Borisova L.G. & Rudicheva L.M. 1968. The use of special features of natural synoptic seasons in making monthly weather forecasts. *Trudy Gidrometeorologicheskogo Nauchno-Issledovatelskogo Centra SSSR* 12: 12–18. [In Russian with English summary].

Brönnimann S., Stickler A., Griesser T., Fischer A.M., Grant A., Ewen T., Zhou T., Schraner M., Rozanov E. & Peter T. 2009. Variability of large-scale atmospheric circulation indices for the northern hemisphere during the past 100 years. *Meteorol. Zeitschrift* 18: 379–396.

Bukantis A. & Bartkevičienė G. 2005. Thermal effects of the NAO impact in the cold period of the year in Lithuania. *Climate Research* 28: 221–228.

Castro-Dýez Y., Pozo-Vazquez D., Rodrigo F.S. & Esteban-Parra M.J. 2002. NAO and winter temperature variability in southern Europe. *Geophys. Res. Lett.* 29: 1160–1164.

Degirmendzic J., Kozuchowski K. & Zmudzka E. 2004. Changes of air temperature and precipitation in Poland in the period 1951–2000 and their relationship to atmospheric circulation. *J. Climatol.* 24: 291–310.

Deser C., Walsh. J.E. & Timlin M.S. 2000. Arctic sea ice variability in the context of recent atmospheric circulation trends. *J. Climate 13*: 617–633.

Efimov V.V., Shokurov M.V. & Barabanov V.S. 2002. Statistical modeling of monthly anomalies of atmospheric precipitations for the region of the Ukraine and Black Sea. *Physical Oceanography* 12: 10–23.

Fyfe J.C., Boer G.J. & Flato G.M. 1999. The Arctic and Antarctic oscillations and their projected changes under global warming. *Geophys. Res. Lett.* 26: 1601–1604.

Hilmer M. & Jung T. 2000. Evidence for a recent change in the link between the North Atlantic Oscillation and Arctic sea ice export. *Geophys. Res. Lett.* 27: 989–992.

Girs A.A. & Kondratovich K.V. 1978. *Methods for long-term weather forecasts*. Gidrometeoizdat, Leningrad. [In Russian with English summary].

Harnik N. & Chang E.K.M. 2002. Storm track variations as seen in radiosonde observations and reanalysis data. *J. Climate* 16: 480–495.

Honda M., Inoue J. & Yamane S. 2009. Influence of low Arctic sea ice minima on anomalously cold Eurasian winters. *Geophys. Res. Lett.* 36: L08707, doi:10.1029/2008GL037079.

Hurrell J.M. & van Loon H. 1997. Decadal variations in climate associated with the North Atlantic Oscillation, *Climatic Change* 36: 301–326.

IPCC 2007. *Climate change. The physical science basis*. Cambridge University Press, Cambridge, UK.

Jaagus J. 2009 Regionalisation of the precipitation pattern in the Baltic Sea drainage basin and its dependence on large-scale atmospheric circulation. *Boreal Env. Res.* 14: 31–44.

Jaagus J., Briede A., Rimkus E. & Remm K. 2010. Precipitation pattern in the Baltic countries under the influence of large-scale atmospheric circulation and local landscape factors. *Int. J. Climatol.* 30: 705–720.

Jacobeit J., Rathmann J. & Philipp A. 2009. Central European temperature and precipitation extremes in relation to large-scale atmospheric circulation types. *Meteorol. Zeitschrift* 18: 397–410.

Jahnke-Bornemann A. & Brümmer B. 2009. The Iceland-Lofotes pressure difference*:* different states of the North Atlantic low pressure zone. *Tellus* 61A: 466–475.

Jamison N. & Kravtsov S. 2010. Decadal variations of North Atlantic sea-surface temperature in observations and CMIP3 simulations. *J. Climate* 23: 4619–4636.

Jones P.D. & Lister D.H. 2009. The influence of the circula-

tion on surface temperature and precipitation patterns over Europe. *Climates of the Past* 5: 259–267.

Kendall M. 1975. *Multivariate analysi*s. Charles Griffin & Company, London.

Kim K.-Y. & Wu Q. 1999. A comparison study of EOF techniques: analysis of nonstationary data with periodic statistics. *J. Climate* 12: 185–200.

Krichak S.O. & Alpert P. 2005. Signatures of the NAO in the atmospheric circulation during wet winter months over the Mediterranean region. *Theor. Appl. Climatol.* 82: 27–39.

Kryjov V.N. 2004. Searching for circulation patterns affecting North Europe annual temperature. *Atmospheric Science Letters* 5: 23–34.

Kutiel H., Maheras P. & Guika S. 1996. Circulation indices over the Mediterranean and Europe and their relationship with rainfall conditions across the Mediterranean. *Theor. Appl. Climatol.* 54: 125–138.

Kutiel H. & Benaroch Y. 2002. North Sea–Caspian Pattern (NCP) — an upper level atmospheric teleconnection affecting the eastern Mediterranean: identification and definition. *Theor. Appl. Climatol.* 71: 17–28.

Niedźwiedź T., Twardosz R. & Walanus A. 2009. Long-term variability of precipitation series in east central Europe in relation to circulation patterns. *Theor. Appl. Climatol.* 98: 337–350.

Overland J.E. & Wang M. 2010. Large-scale atmospheric circulation changes are associated with the recent loss of Arctic sea ice. *Tellus* 1A: 1–9.

Panagiotopoulos F., Shahgedanova M., Hannachi A. & Stephenson D. 2005. Observed trends and teleconnections of the Siberian High: a recently declining center of action. *J. Climate* 18: 1411–1422.

Philipp A., Della-Marta P.M., Jacobeit J., Fereday D.R., Jones P.D., Moberg A. & Wanner H. 2007. Long-term variability of daily North Atlantic–European pressure patterns since 1850 classified by simulated annealing clustering. *J. Climate* 20: 4065–4095.

Pekarova P., Miklanek P. & Pekar J. 2006. Long-term trends and runoff fluctuations of European rivers climate variability and change — hydrological impacts. *IAHS Publ.* 308: 520–525.

Polonsky A. & Basharin D. 2002. On an influence of North Atlantic and El-Nino Southern Oscillations on the air temperature variability over the European-Mediterranean region. *Izvestija. RAN, seriya Fizika Atmosfery i Okeana* 38: 135–145. [In Russian with English summary].

Polonsky A. [Полонски А.] 2008. [*The role of the ocean in climate change*]. Naukova Dumka, Kiev. [In Russian].

Polonsky A., Basharin D. & Stankunavicius G. 2011. Comparison of the climate variability of the surface air temperature between observation and results of climate's model estimation: regional and global scales. In: Ivanov V.A. (ed.), *Ecological safety of the coastal and shelf zones and comprehensive use of shelf resources: collected scientific papers*, vol. 24, NAS of Ukraine, MGI, Sevastopol, pp. 142–150. [In Russian with English summary].

Rogers, J.C. 1997. North Atlantic storm track variability and its association to the North Atlantic Oscillation and climate variability of northern Europe. *J. Climate* 10: 1635–1647.

Rudolf B., Becker A., Schneider U., Meyer-Christoffer A. & Ziese M. 2011. New GPCC full data reanalysis version 5 provides high-quality gridded monthly precipitation data. *GEWEX News* 21: 4–5.

Savelieva N.I., Semiletov I., Weller G.E., Vasilevskaya L.N. & Yusupov V.I. 2004. Climate change in the northern Asia in the second half of the 20th century. *Pacific Oceanography* 2: 74–84.

Seierstad I.A., Stephenson D.B. & Kvamsto N.G. 2007. How useful are teleconnection patterns for explaining variability in extratropical storminess? *Tellus* 59A: 170–181.

Sizov A.A. & Chekhlan A.E. 2007. Water temperature anomalies in the north Atlantic and precipitation in the Crimea in the years with extreme values of the north Atlantic oscillation index. *Russian Meteorology and Hydrology* 32: 54–59.

Slonsky V. & Yiou P. 2002. Does the NAO index represent zonal flow? The influence of the NAO on North Atlantic surface temperature. *Climate Dyn.* 19: 17–30.

Stankūnavičius G. 2009. The long range predictability of the temperature and precipitation anomalies in Lithuania. *Geografija* 45: 33–43. [In Lithuanian with English summary].

Stephenson D.B., Pavan V., Collins M., Junge M.M. & Quadrelli R. 2006. North Atlantic Oscillation response to transient greenhouse gas forcing and the impact on European winter climate: a CMIP2 multi-model assessment. *Clim. Dyn.* 27: 401–420.

Straus D. & Krishnamurthy V. 2007. The preferred structure of the interannual Indian monsoon variability. *Pure and Applied Geophysics* 164: 1–16.

Thompson D.W.J., Wallace J.M. & Hegerl G.C. 2000. Annular modes in the extratropical circulation. Part II: Trends. *J. Climate* 13: 1018–1036.

Tomozeiu R., Stefan S. & Busuioc A. 2005. Winter precipitation variability and large-scale circulation patterns in Romania. *Theor. Appl. Climatol.* 81: 193–201.

Trigo I.F. 2005. Climatology and interannual variability of storm-tracks in the Euro-Atlantic sector: a comparison between ERA-40 and NCEP/NCAR reanalyses. *Clim. Dyn.* 26: 127–243.

Turkes M. 1998. Influence of geopotential heights, cyclone frequency and southern oscillation on rainfall variations in Turkey. *Int. J. Climatol.* 18: 649–680.